



An experimentally-accurate and complete room-temperature infrared HCN line-list for the HITRAN database



Georg Ch. Mellau, Dr.^a, Vladimir Yu. Makhnev^{b,*}, Iouli E. Gordon, Dr.^c, Nikolay F. Zobov, Dr.^b, Jonathan Tennyson, Professor^d, Oleg L. Polyansky, Dr.^{b,d,b}

^a Physikalisch-Chemisches Institut, Justus-Liebig-Universität Gießen, Heinrich-Buff-Ring 17, Gießen D-35392, Germany

^b Institute of Applied Physics, Russian Academy of Sciences, 46 Ulyanov Street, Nizhny Novgorod 603950, Russia

^c Harvard-Smithsonian Center for Astrophysics, Atomic and Molecular Physics Division, 60 Garden St, Cambridge, MA, USA

^d Department of Physics and Astronomy, University College London, Gower Street, London WC1E 6BT, United Kingdom

ARTICLE INFO

Article history:

Received 28 February 2021

Revised 23 March 2021

Accepted 23 March 2021

Available online 8 April 2021

Keywords:

HCN

Hydrogen cyanide

Molecular spectra

Infrared spectra

HCN line list

ABSTRACT

A hydrogen cyanide line list (MOMeNT-90) developed for the HITRAN spectroscopic database covering 0–7500 cm⁻¹ range ($\lambda > 1330$ nm) is presented. The line list is a combination of the variationally calculated line intensities with line centers obtained from experimentally derived energy levels. There are four features of this line list which distinguishes it from the previously calculated ones. First, the intensities are variationally calculated using a new, high-accuracy potential energy surface (PES) obtained via fitting the PES using experimental energy levels. Second, a new *ab initio* dipole moment surface was calculated at a high level of quantum chemical theory. Based on the wave functions calculated with the new PES and use of the new dipole moment surface, line intensities are reported which of similar accuracy to those obtained experimentally. Third, the calculated states are mapped to the existing complete set of experimental eigenenergies, resulting in an assigned and complete HCN line list down to the HITRAN intensity threshold of 10⁻³⁴ cm/molecule. Fourth, extensive validation of the line list is provided through line-by-line comparisons of the results with measured HCN spectra which confirms the accuracy of the intensities used to construct the line list. The line list is augmented with parameters needed to calculate line widths for pressure-dependent simulations.

© 2021 Elsevier Ltd. All rights reserved.

1. Introduction

Hydrogen cyanide (HCN) is a trace atmospheric species and is present in the atmosphere mainly as a product of biomass burning. Atmospheric HCN concentration is a clear indicator of forest fires [1]. Combating forest fires is an important aspect in the fight against global warming. Accurate spectroscopic line lists are required for atmospheric HCN concentration monitoring.

HCN is an important astrophysical species. In the solar system it has been detected in the atmospheres of gas giants [2,3] and Saturn's moon Titan [4] as well as comets [5–7]. Interstellar HCN is well-known [8], and it forms an important component of the atmosphere of cool stars [9,10] and circumstellar disks [11]. Recently HCN has been detected in a number of exoplanets [12–14].

The temperature of the molecular gas determines the type of line list required for an analytic-type spectroscopic analysis. Thus, there are “cold” (room temperature) line lists such as HITRAN

[15] or GEISA [16] and “hot” line lists such as HITEMP [17,18] or ExoMol [19]. Ideally, the data used to produce a line list originate from high-precision, high-resolution spectroscopic measurements. Due to the sheer number of the transitions required, this is often not possible. As a result many line lists are a combination of experimental data sets and calculated *ab initio* predictions.

The first *ab initio* calculation of HCN band strength was performed by Jørgensen et al. [20] who generated an *ab initio* line list for hot HCN which they used for stellar modeling [9]. An improved line list by Harris et al. [21] was based on the *ab initio* potential energy surface (PES) and dipole moment surface (DMS) of Van Mourik et al. [22]. The *ab initio* dataset covers all states of the [H,C,N] molecular system up to the isomerization barrier with a typical error for low *J* rovibrational transitions of 1–20 cm⁻¹ [23]. Subsequent line lists [24–26] have improved the original line list of Harris et al. by replacing calculated energy levels with available empirical or experimental energy levels.

The best *ab initio* HCN rovibrational eigenenergies based on the Born–Oppenheimer (BO) approximation with all possible correction terms are still not accurate enough for the needs of the sci-

* Corresponding author.

E-mail address: makhnev@ipfran.ru (V.Yu. Makhnev).

tific community using spectroscopy as an analytical tool. For small molecules, it is not a problem to use experimental spectroscopy to detect the fundamental vibrations and also many of the rovibrational states with a few quanta of vibrational excitation. Absorption spectroscopy with a very long path length or at high temperature can extend the range of vibrational and rotational excitation covered by experiment, but complete coverage of the eigenenergy ladder remains difficult to achieve with this spectroscopic technique.

In 1997, one of us [28,29] showed that a special setup of a tube furnace type emission experiment, referred to as HOT GAs Molecular Emission (HOTGAME) spectroscopy, can cover the complete eigenenergy ladder of triatomic molecules such as HCN or CO₂. The analysis of his first set of HCN/HNC spectra was performed using the spectroscopic programs and techniques available at that time [30–32]. The HOTGAME emission spectra are very dense and sample an extremely large dynamic range of line intensities. To extract both the transitions between the very highly excited states, and to obtain accurate line positions as well as intensities for the assigned lines, a dedicated analysis program was developed [33].

After further significant improvement of the experiment sensitivity, Mellau introduced the concept of an experimental “Complete set of eigenenergies” for HCN and HNC [23,34]. This refers to a complete list of experimental eigenstates with an relative accuracy of better than 10⁻⁸, where “complete” means that not a single eigenenergy is missing from the set up to a certain highly excited cutoff eigenenergy value. These original data sets were extended with additional band series [35,36]. The line list reported in this work are based on these HCN molecular eigenenergy lists.

Recently, some of us have constructed an HCN PES capable of predicting HCN infrared transitions with an accuracy of about 0.037 cm⁻¹ [37], about two orders of magnitude better than the original calculations of van Mourik et al. In this paper, a further improvement of the PES by a factor of about 3 is described. This improvement is based on theoretical insights gained by mapping the experimental eigenenergies with the *ab initio* data. In this work, we combine the intensities obtained with our greatly improved PES and DMS with the experimental energy levels to provide a spectroscopically accurate line list for HCN.

The paper is organized as follows. In the [Section 2](#) we present the details of the PES calculation. In the [Section 3](#) we describe the *ab initio* calculations of the line intensities of our line list which we call var-MOMeNT-90. In the [Section 4](#) the mapping of experimental eigenenergy states to the *ab initio* data set is described. In the [Section 5](#) the resulting MOMeNT-90 line list is described. In the [Section 6](#) the validation procedure of the line list is described. In the [Section 7](#) the linewidths, supplemented to the line list, are described. In the final [Section 8](#) we give our concluding remarks and an outlook of the oncoming work

2. HCN potential energy surface (PES)

As a starting point of the fit of the PES to experimental energy levels we used the *ab initio* surface obtained in Makhnev et al. [38]. This PES was based on MRCI+P-r energies (multi-reference configuration interaction with Pople correction, relaxed reference) computed with an aug-cc-pCV6Z basis set. Only such an extensive basis set could provide a good starting point for a fit of the experimental levels.

2.1. Non-adiabatic effects on HCN spectrum

There are two mass-dependent corrections to Born–Oppenheimer approximation: BODC (Born–Oppenheimer Diagonal Correction, or adiabatic correction) and non-adiabatic correction. An adiabatic correction has been already determined for HCN

Table 1

Input parameters for DVR3DRJZ module of DVR3D [27]; the Morse parameters are in atomic units, atomic masses are in Da.

Parameter	Value	Description
NPNT1	40	Number of r_1 radial DVR points (Gauss–Laguerre)
NPNT2	40	Number of r_2 radial DVR points (Gauss–Laguerre)
NALF	50	Number of angular DVR points (Gauss–Laguerre)
NEVAL	950	Number of eigenvalues/eigenvectors required
MAX2D	2750	Dimension of 2D vibrational Hamiltonian
MAX3D	3500	Dimension of final vibrational Hamiltonian
XMASS (H)	1.007276	Mass of hydrogen atom
XMASS (C)	12.000000	Mass of carbon atom
XMASS (N)	14.003074	Mass of nitrogen atom
r_{1e}	2.3	Morse parameter (r_1 radial basis function)
D_{1e}	0.1	Morse parameter (r_1 radial basis function)
ω_{1e}	0.0105	Morse parameter (r_1 radial basis function)
r_{2e}	3.2	Morse parameter (r_2 radial basis function)
D_{2e}	0.1	Morse parameter (r_2 radial basis function)
ω_{2e}	0.004	Morse parameter (r_2 radial basis function)

molecule in the recent work on *ab initio* potential energy surfaces [38].

Non-adiabatic corrections for HCN, or indeed other small molecules, are harder to characterize and therefore more rarely considered. We investigated inclusion of this correction previously [37,38] as they proved necessary to achieve a good fit of the empirical energy levels up to $J = 10$; with them these levels were reproduced with a standard deviation of $\sigma = 0.0373 \text{ cm}^{-1}$.

However, at the start of this project we compared the HCN energy level predictions for $J > 20$ with empirical ones due to Mellau et al. [23,39] and noticed that rotational part of energy deviates from the experimental value for each state in a systematic manner. We suspected that this behavior was caused by our attempt to improve our energies by including a non-adiabatic correction using both atomic masses in the calculation and as part of the fit itself. This hypothesis led us to try to fit levels without making full use of the non-adiabatic correction on the assumption that these both components are not consistent with each other and their effect should be reduced. We used the nuclear mass for the hydrogen atom and retained atomic masses for the carbon and nitrogen atoms. This combination was used because the hydrogen mass plays the main role in non-adiabatic correction to rotational-vibrational states.

2.2. Nuclear motion calculations

Vibrational energy levels were calculated using the DVR3D program suite [27]. The parameters used are presented in [Table 1](#); Morse-like oscillators were used for the radial basis functions. We include almost all corrections used in the *ab initio* PES: adiabatic and relativistic correction surfaces and a nonadiabatic correction (by choosing atomic masses), to get the best starting point for fitting. More details about corrections are given in Ref. [38].

2.3. Potential energy surface fitting

Our approach has already been described in detail [37]. Our fit started from the *ab initio* data of Ref. [38] fitted to a polynomial form:

$$V_{\text{ai}}^{\text{HCN}}(r_1, r_2, \theta) = \sum_{ijk} b_{ijk} s_1^i s_2^j s_\theta^k. \quad (1)$$

$s_1 = r_1 - r_{1e}^{\text{HCN}}$,
 $s_2 = r_2 - r_{2e}^{\text{HCN}}$, where r_1 is the CH bond length, r_2 is the CN bond length and θ is H–C–N angle (likewise, as defined in Makhnev et al. [37]), and $(r_{1e}^{\text{HCN}}, r_{2e}^{\text{HCN}}, \theta_e^{\text{HCN}})$ corresponds to the

Table 2

HCN vibration energy levels. Experimental values from work of Mellau [23]. All values are in cm^{-1} .

State	Obs.	Calc.	Obs.-Calc. (this work)	Obs.-Calc. [37]
(0 2 0)	1411.413	1411.431	-0.017	-0.035
(0 0 1)	2096.845	2096.868	-0.023	-0.042
(0 4 0)	2802.958	2802.963	-0.004	-0.030
(1 0 0)	3311.477	3311.484	-0.007	-0.005
(0 2 1)	3502.121	3502.117	0.003	-0.001
(0 0 2)	4173.070	4173.100	-0.029	-0.071
(0 6 0)	4174.608	4174.601	0.007	0.013
(1 2 0)	4684.310	4684.323	-0.013	-0.029
(0 4 1)	4888.039	4888.052	-0.012	-0.033
(1 0 1)	5393.697	5393.689	0.008	-0.013
(0 8 0)	5525.812	5525.824	-0.012	0.013
(0 2 2)	5571.734	5571.722	0.012	0.021
(1 4 0)	6036.960	6036.968	-0.008	-0.019
(0 0 3)	6228.598	6228.601	-0.003	-0.064
(0 6 1)	6254.405	6254.401	0.004	-0.056
(2 0 0)	6519.610	6519.612	-0.001	-0.011
(1 2 1)	6760.705	6760.729	-0.023	-0.037
(0 10 0)	6855.443	6855.429	0.013	-0.058
(0 4 2)	6951.683	6951.723	-0.040	-0.053
(1 6 0)	7369.443	7369.453	-0.010	0.041
(1 0 2)	7455.423	7455.390	0.033	-0.021

equilibrium configuration of HCN (we retain HCN superscripts here for the consistency with paper [37] where both HCN and HNC systems are considered.). This fit to *ab initio* data (900 points, 54 constants, see [37] for details) gives a standard deviation of about 1.5 cm^{-1} , which can be compared to the fit global covering both HCN and HNC wells performed in Makhnev et al. [38], which gave a standard deviation of about 2.6 cm^{-1} .

$V_{\text{ai}}^{\text{HCN}}(r_1, r_2, \theta)$ provides the starting point for a fit to the observed HCN energy levels:

$$V(r_1, r_2, \theta)^{\text{HCN}} = V_{\text{ai}}^{\text{HCN}}(r_1, r_2, \theta) + \sum_{ijk} d_{ijk} s_1^i s_2^j s_\theta^k. \quad (2)$$

We took $(r_{1e}, r_{2e}, \theta_e) = (1.066 \text{ \AA}, 1.153 \text{ \AA}, 180.0^\circ)$ as the minimum in the HCN well from the *ab initio* PES. Mellau [23] reported experimental characterization of all 3822 eigenenergies of HCN up to 6880 cm^{-1} relative to the ground state using high temperature hot gas emission spectroscopy. These data set was used in this work to fit the PES. The set of *ab initio* polynomial coefficients from Eq. (2) is presented in the Ref. [37], the set of optimized polynomial coefficients from Eq. (2) is presented in the Supplementary Material (Table 1).

2.4. Accuracy of the fitted potential

As shown below, significant improvement in both vibrational and rovibrational energy levels reproduction has been achieved. In particular, vibrational energy values were reproduced with a standard deviation $\sigma = 0.0172 \text{ cm}^{-1}$ (see Table 2). The standard deviation for energy levels for the J s included to fit (0, 2, 5, 9) roughly corresponds with the vibrational one. There are two reasons for this: the nature of the fit itself and the weak contribution of the rotational non-adiabatic correction to the vibrational levels.

The deviation from the experimental levels with $J > 10$ grows with J . Some high vibrational-rotational levels can deviate from the experiment by about 1 cm^{-1} . Even taking into account the fact that the nonadiabatic correction still requires improvement, it is worth noting such an unprecedented level of predictive ability of the highly excited ro-vibrational states of the new PES.

3. The var-MOMeNT-90 HCN line list

The var-MOMeNT-90 HCN line list is built on our new spectroscopically-detemined PES. This PES reproduces the low J ex-

Table 3

HCN rovibration energy levels. Experimental values from work of Mellau [23]. All values are in cm^{-1} .

J	σ [37]	σ (this work)	N_{levels}
0	0.0382	0.0172	21
0&2	0.0312	0.0133	90
0&2&5	0.0287	0.0121	199
0&2&5&9	0.0330	0.0166	322
0&2&5&9&10	0.0373	0.0175	445
0&2&5&9&10&20	0.0926	0.0340	568

perimental energy levels of hydrogen cyanide with a standard deviation $\sigma = 0.0121 \text{ cm}^{-1}$ (for levels with $J = 0, 2$ and 5, see Table 3 for more details). A fitted PES is important not only for the accuracy of the line positions, but also for the accuracy of the line intensities [40]. There is a difference of few percents between the line intensities obtained using a pure *ab initio* PES and the same PES but spectroscopically tuned [37].

The spectroscopically tuned PES was used together with the new *ab initio* DMS previously reported [37] to calculate the line centers and line intensities using the DVR3D program suite [27]. The *ab initio* DMS was created for the HCN well to cover all transitions between the energy levels in the $0\text{-}7200 \text{ cm}^{-1}$ eigenenergy range. An aug-cc-pCV5z basis set with the Pople relaxed correction and a relativistic correction, mass-velocity plus first-order Darwin term (MVD1) were used to construct the new DMS.

For all fundamental transitions the DMS reproduces the measurements better than the previous work of van Mourik et al. [22]. The accuracy of the calculated line intensities for two of the fundamental transitions is about 1%, this is within the experimental uncertainties of very accurate experimental intensity measurements. Since the line list for this work was constructed for the eigenenergy range $0\text{-}7200 \text{ cm}^{-1}$, some transitions involving eigenstates in the $7200\text{-}10,300 \text{ cm}^{-1}$ range may be less accurate.

The final *ab initio* line list was prepared for the 296 K HITRAN temperature with an intensity cutoff at $10^{-34} \text{ cm}/\text{molecule}$. In the calculations $J_{\text{max}} = 90$ was used, but due to the selected sensitivity of the cold line list, the transitions present in the list have J quantum numbers well below the $J = 90$ limit. On the other hand, this means that none of the bands is limited at high J due to the incompleteness of the data set, the limit is always given by the cutoff sensitivity of the line list.

The overall comparison between the HITRAN2016 database [15] and the *ab initio* line list of this work is shown in Figs. 1 and 2.

4. Mapping the experimental data to the *ab initio* data

A one-to-one mapping between the experimental and the *ab initio* sets of energy levels is possible only after expanding the good quantum numbers used to label the *ab initio* eigenenergies with approximate vibrational quantum numbers. Matching between the data sets with a search for the nearest neighbor seems to be straightforward if one considers only the accuracy of the theoretical pure vibrational eigenenergies. However, this is actually a fallacy; even for the pseudo-theoretical eigenenergy list reported in this paper, such matching is not possible. With rotational excitation, this accuracy deteriorates by several orders of magnitude and the density of states increases considerably due to the sub-states with non-zero vibrational angular momentum.

In this work, we have used a universal mapping method developed in Mellau [23] that is based on the spectroscopic patterns of molecular eigenenergies. In an ongoing research project, this method is being implemented in Giessen as a computational package. The idea behind this project is to obtain an immedi-

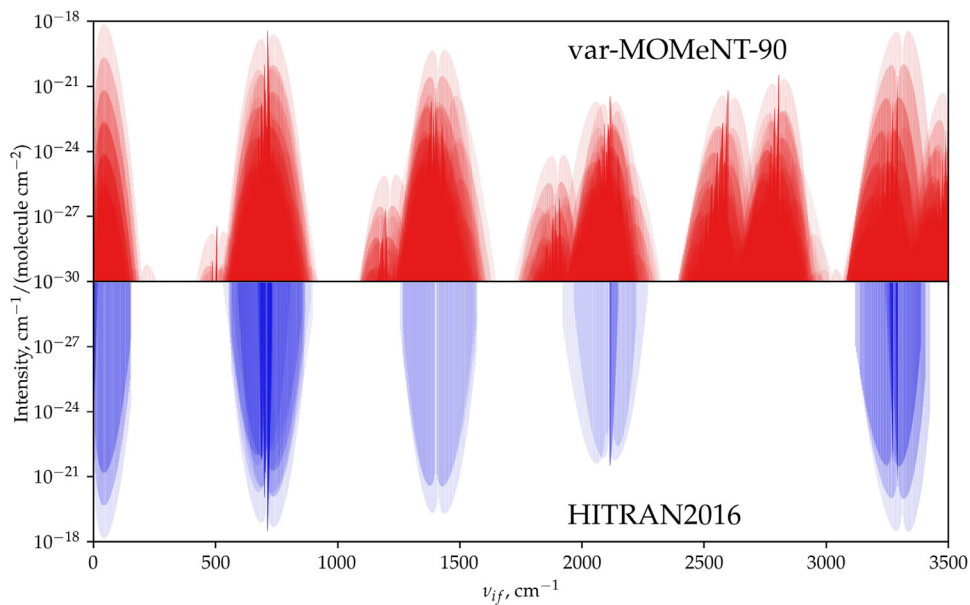


Fig. 1. Comparison of the variational var-MOMeNT-90 line list of this work and HITRAN2016 in the 0–3500 cm^{-1} region.

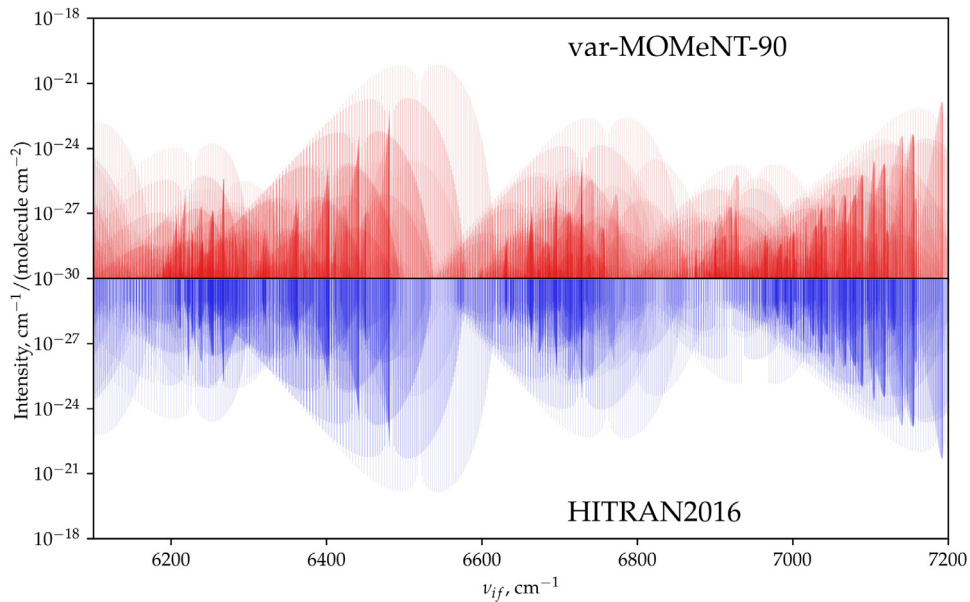


Fig. 2. Difference between the line-list “var-MOMeNT-90” and HITRAN2016 edition in the 6100–7200 cm^{-1} region.

ate and fully automatic response to the quality of any molecular physics theory that computes a complete set of eigenenergies for a molecular system. The response is a high quality visualisation of the differences between measurement and theory. As described in Section 2.1, the first visualisation output of the differences for the eigenenergies calculated with the initial PES allowed us to significantly improve the fitted PES and eigenenergy calculations (see differences between the two σ of the last row of the Table 3).

As a first application, the eigenenergy data set calculated in this work was mapped onto the experimental HCN data set for all vibrational states up to 10,300 cm^{-1} . The result of this analysis is a $J = \ell, \dots, 90$ manifold of *ab initio* and experimental pair of rovibrational eigenenergies. For each vibrational state the experimental eigenenergies were extrapolated from the state-specific J_{\max} detected in the spectrum to $J = 90$ with the state specific spectroscopic constants. A few vibrational states within the 7000–10,300 cm^{-1} eigenenergy wavenumber range were not mea-

sured; for these bands spectroscopically predicted eigenenergies [23,41] were mapped to the *ab initio* data.

This complete rovibrational data set was used to generate the HCN line list.

5. The MOMeNT-90 HCN line list

This paper provides a line list for transitions that are missing from the HITRAN database or improve the line intensities present in the HITRAN2016 database. Our data set is limited first by the 10,300 cm^{-1} cutoff of the vibrational energies considered in this work. The second limitation is related to the sensitivity cutoff used in generating the pure *ab initio* line list, this was set for this work to $10^{-34} \text{ cm/molecule}$. We have excluded from the line list some of the vibrational states predicted only spectroscopically.

After mapping the experimental data set to the theoretical one, spectroscopically defined band series were extracted from the data

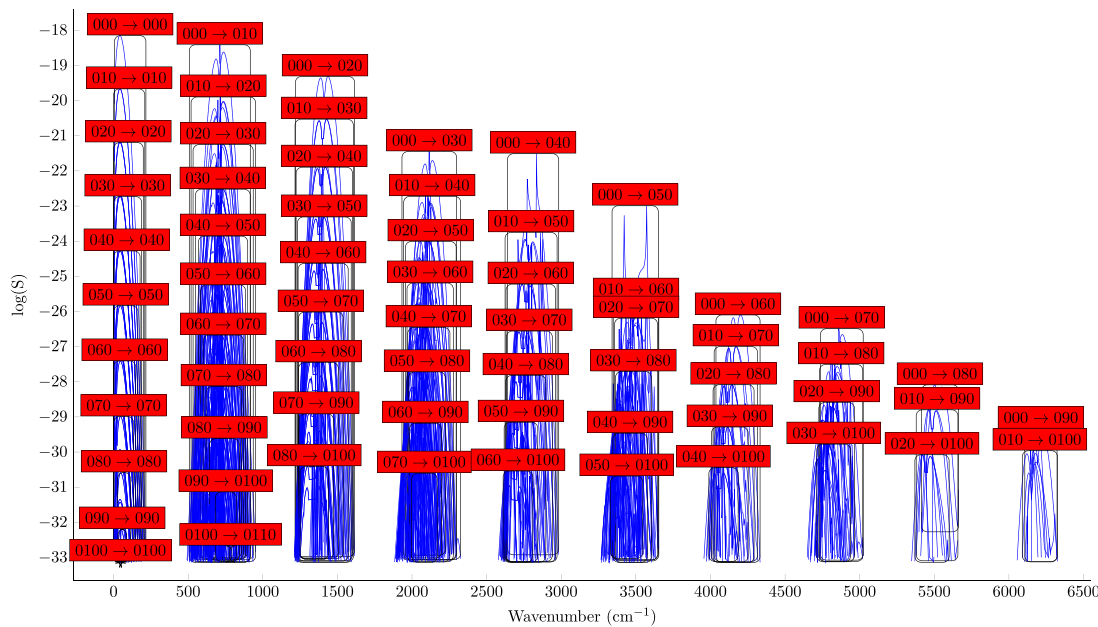


Fig. 3. Overview of the $0v_2^0 \rightarrow 0(v_2 + \Delta v_2)^0$ line list.

set. This allows a more precise control of the data and the validation of the data set band by band.

The natural way to partition the set of HCN molecular transitions is to fix the stretching quantum numbers v_1 and v_3 for the lower and upper states, respectively, and consider all possible transitions matching such a setting. The reported transitions are thus split into data files containing all transitions between states with fixed stretching quantum numbers v_1 and v_3 .

The results are reported in two sets of line list files. One set contains the continuous list of line data for a given vibrational series. These files are named MAPDATA and can be imported directly by user analysis programs.

The same data are presented in a second file organized into spectroscopic bands. These files are named MAPRESULT and can be used for spectroscopic band-by-band analysis of HCN spectra. The bands in these files were mapped to the HITRAN database, and the transition present in HITRAN are listed directly below the lines containing the data of this work. The MAPDATA and MAPRESULT files are part of the supplementary data published with this work.

If a line is present in HITRAN, a final column is added with the difference between the line position compiled in this work and the line position from the HITRAN database. For a large portion of the bands compiled in this work that are also present in HITRAN, this column lists 0.00000 values for all band lines. These transitions appear to have already been compiled for HITRAN with the Mellau eigenenergy tables used also in this work, a reference to the corresponding experimental papers appears to be missing from the HITRAN2016 database.

Figs. 3, 4, 5 show the overview plot for the subbands of three MAPDATA files. The highest line intensity of the bands are marked by the transition quantum number labels.

6. Validation of the new HCN transition data set

There is a large difference in the number of molecular eigenstates and the number of possible transitions between these states that are relevant for spectroscopic measurements. For a triatomic molecule - and especially for HCN - it is possible to experimentally sample the complete eigenenergy ladder by HOTGAME measurements. Once one has the experimental eigenenergies, it is possi-

ble to calculate any possible transition frequency with experimental accuracy. It is not difficult to see that obtaining a complete set of accurate experimental line intensities for this set of transition frequencies is quite a different problem.

The accuracy of standard experimental intensity analysis is very limited for various technical and chemical reasons. A set of line intensities accurate to 1 percent can be considered an accurate experimental data set. This low relative accuracy, compared to the relative accuracy of 10^{-8} needed to obtain experimental grade results for line position, can be achieved by accurate *ab initio* calculations [42]; transition probabilities can be calculated with an accuracy similar to the majority of experimental results. The only problem here is the validation of the theoretical results.

To validate the theoretical line intensities calculated in this work, we compare simulated spectra with spectra recorded in Gießen. Here we present the comparison with the absorption spectrum labeled AA (a selected part of this spectrum is shown in Fig. 6a), which has already been reported in reference [43]. The line intensities of this absorption spectrum was revisited in reference [44]. In the cited work, the AA absorption spectrum was used to calibrate the intensity axis of some emission spectra. Calibrated emission spectra can be used to extract accurate absolute line intensities. Such an analysis offers the prospect of covering wavenumber regions with a complete set of experimental line intensities, even for hot line lists. The absorption spectrum AA was compared in reference [44] to the intensity measurements of Devy et al. [45]. The result of this analysis was that the effective pressure of the AA experiment is slightly lower than the value measured with the pressure transducer due to the adsorption of the HCN molecules on the metallic surface of the cell.

In order to give an error bar for the observed line intensities, we have to consider two main effects. The temperature of the molecular gas is set to the average temperature in the laboratory during the measurement. The effect of this uncertainty corresponds to an intensity error of at most 1%. The difference between the recorded and the calibrated pressure corresponds to a relative error of the intensities of 8%. By calibrating the pressure, we think that this error is reduced to at least half of this value. We think that the experimental absorption spectrum should match our simulations within 5% (considering the *ab initio* line intensity

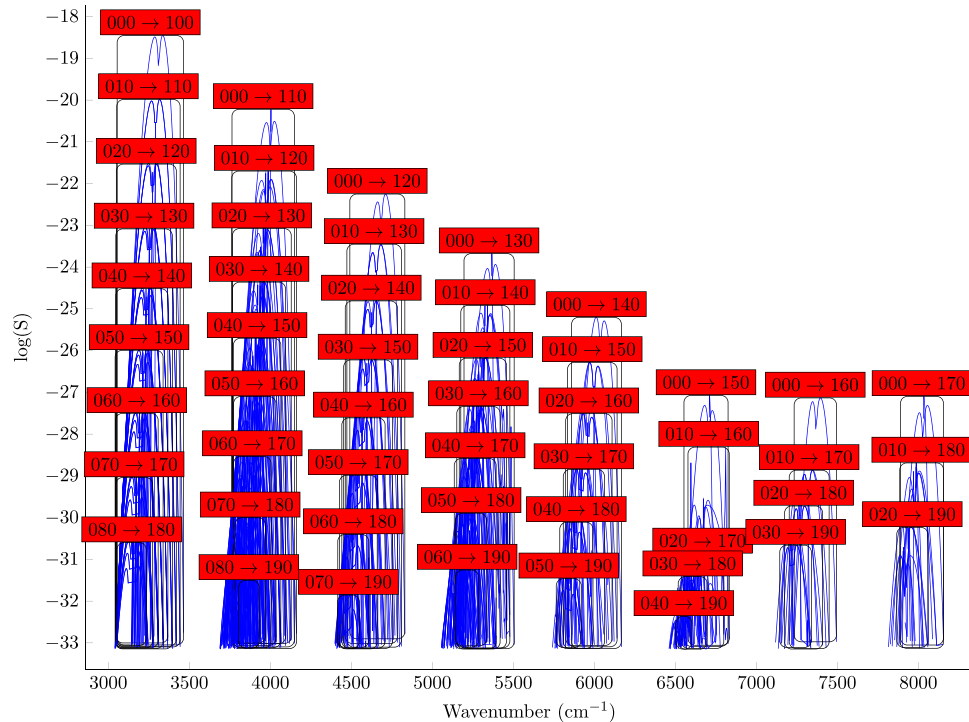


Fig. 4. Overview of the $0\nu_20 \rightarrow 1(\nu_2 + \Delta\nu_2)0$ line list.

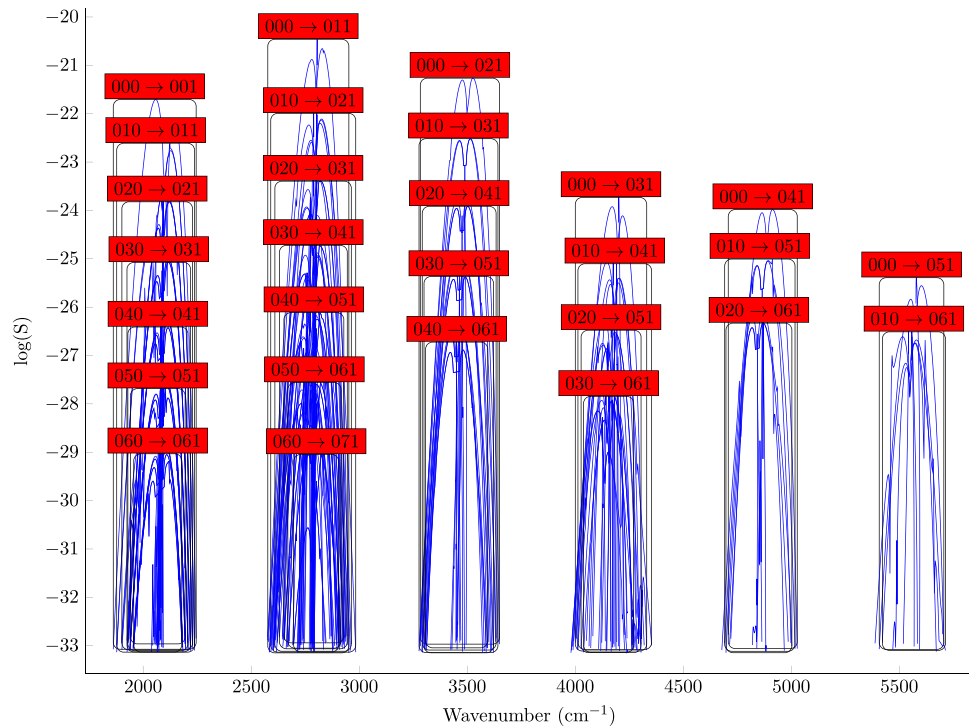


Fig. 5. Overview of the $0\nu_20 \rightarrow 0(\nu_2 + \Delta\nu_2)1$ line list.

parameter error-free) and that this is a conservative estimation of the expected error bar. Pressure calibration was performed independently of the actual measurements.

Fig. 1 is a standard method for comparing line lists. Only basic differences between line lists can be made visible with such a figure. Because of the sheer number of transitions, it is not obvious how to compare line lists or how to compare a line list with a measured spectrum. For example, one can pick the spectral region

of a band and plot a measured spectrum and a simulated spectrum on the same axis. This is still not better, as can be seen in the Fig. 6b. The width of the lines in high resolution spectra is much smaller than the wavenumber spacing between the lines, and thus the experimental and simulated spectra overlap completely.

Fig. 6c shows a possible visualization of a spectroscopic band, a *band plot*. Here, a small region around each line of a subband is selected, and the axis regions between the lines are removed.

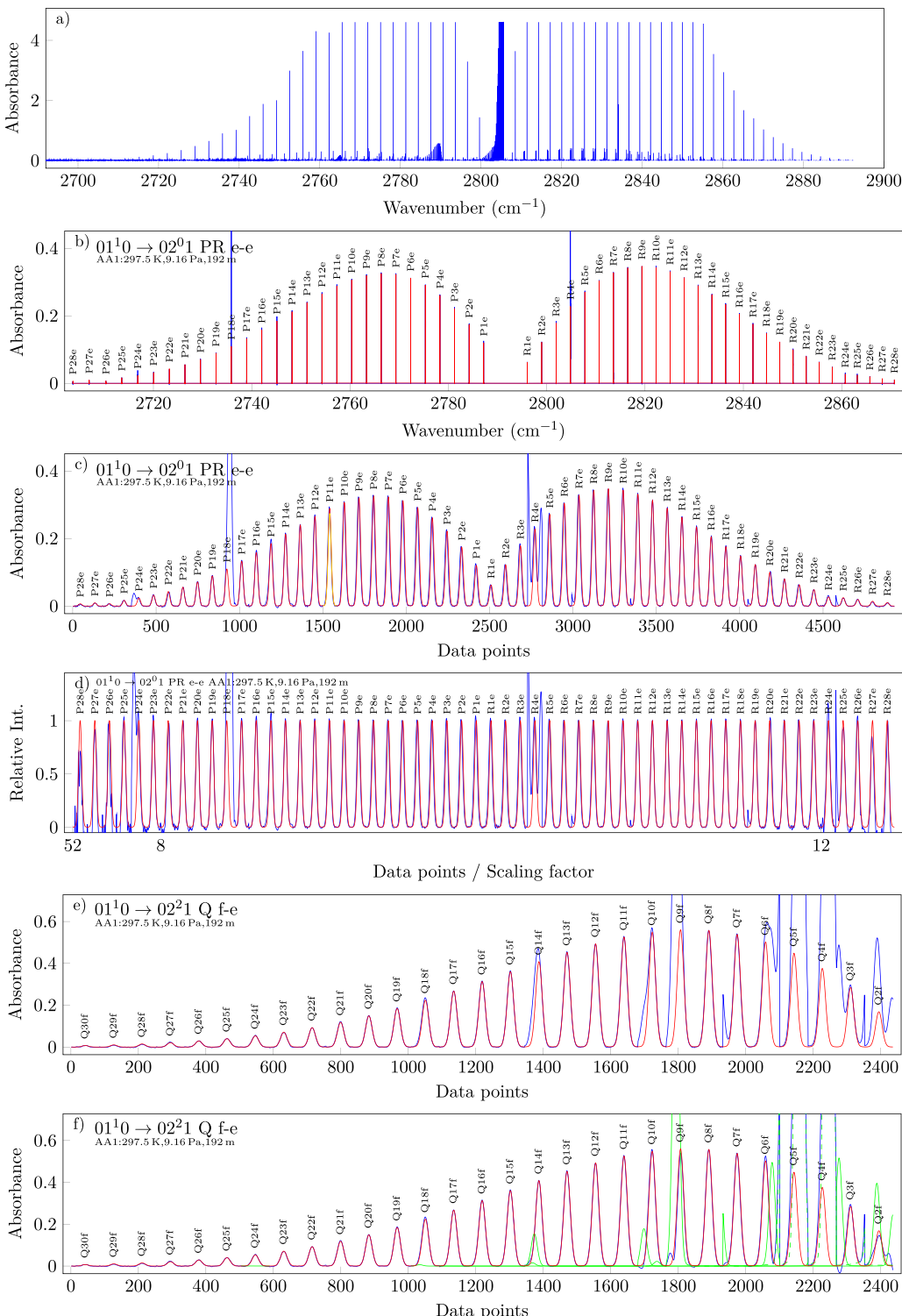


Fig. 6. Line list validation figures: from full spectrum plot (a) to corrected (f) and scaled band plots (d). The band plot figures allow a visual inspection of the quality of the line list. Experimental spectrum is drawn in blue, simulated spectra in red and green. Line P11e is plotted in yellow with an intensity parameter multiplied by 0.95 to facilitate visual estimation of the difference between measured and *ab initio* data. (For interpretation of the references to color in this figure legend, the reader is referred to the web version of this article.)

The band plot allows a quick overview of the intensity agreement between experiment and theory. Here the problem remains that as the intensity of the lines decreases, the comparison becomes less clear.

Fig. 6d shows the same band with the individual lines scaled by individual factors. This figure has now lost all typical band inten-

sity and line spacing structure, but is probably the best visualisation of the intensity match.

Fig. 6e shows another example of a band plot. Here, both low and high intensity lines of other bands overlap with the lines of the selected band. Fig. 6f shows a *corrected band plot*. In this plot, the simulated lines of other bands are shown (green curves) and

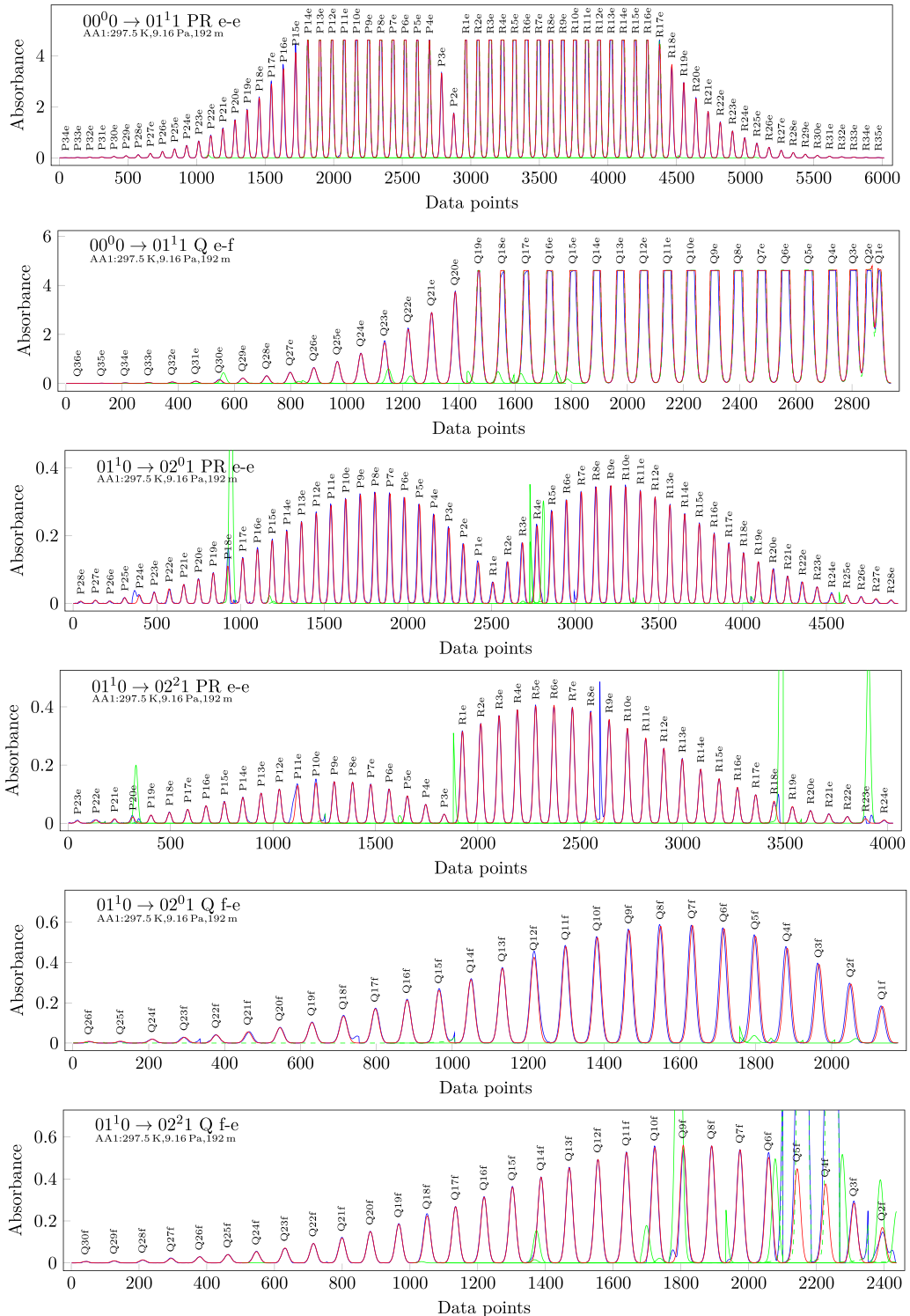


Fig. 7. Comparison between the line list of this work and an FT-IR spectrum. In these band plots, the individual lines of a subband are joined to allow a visual inspection of the line shapes. Experimental spectrum is drawn in blue, simulated spectra in red and green. (For interpretation of the references to color in this figure legend, the reader is referred to the web version of this article.)

these are used to correct the measured spectrum. For the lines labeled Q14, Q10 and Q9, this correction leads to a better intensity match between experiment and theory for the selected band, as expected. For saturated lines such a correction is not possible, in this case the saturated lines of the other bands are drawn dashed.

Figs. 7 and 8 show the corrected band plots of the $0\nu_2 \rightarrow 0(\nu_2 + 1)1$ transitions covering the $2700\text{--}2900\text{ cm}^{-1}$ wavenumber

range. These bands are missing from the HITRAN database. The validation figures show that the match between experiment and our new HCN line list is better than 5%.

Figs. 9 and 10 show the corrected band plots of the $0\nu_2 \rightarrow 1(\nu_2 + 1)0$ transitions covering the $3150\text{--}3450\text{ cm}^{-1}$ wavenumber range. These bands have been partially included in the HITRAN2016 database. The validation figures show that for the fun-

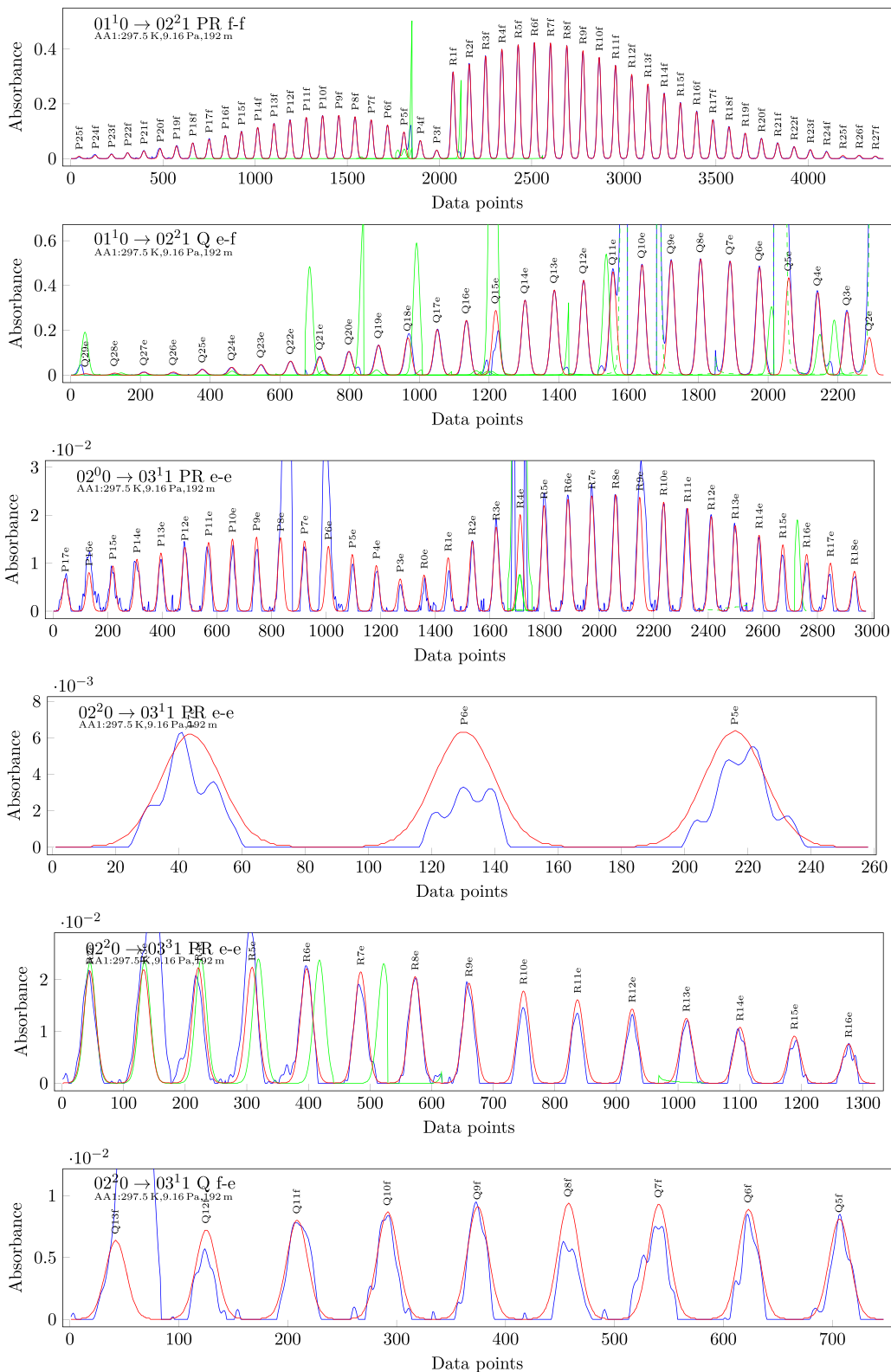


Fig. 8. Comparison between the line list of this work and an FT-IR spectrum. In these band plots, the individual lines of a subband are joined to allow a visual inspection of the line shapes. Experimental spectrum is drawn in blue, simulated spectra in red and green. This figure shows some of the weak bands at the noise level. (For interpretation of the references to color in this figure legend, the reader is referred to the web version of this article.)

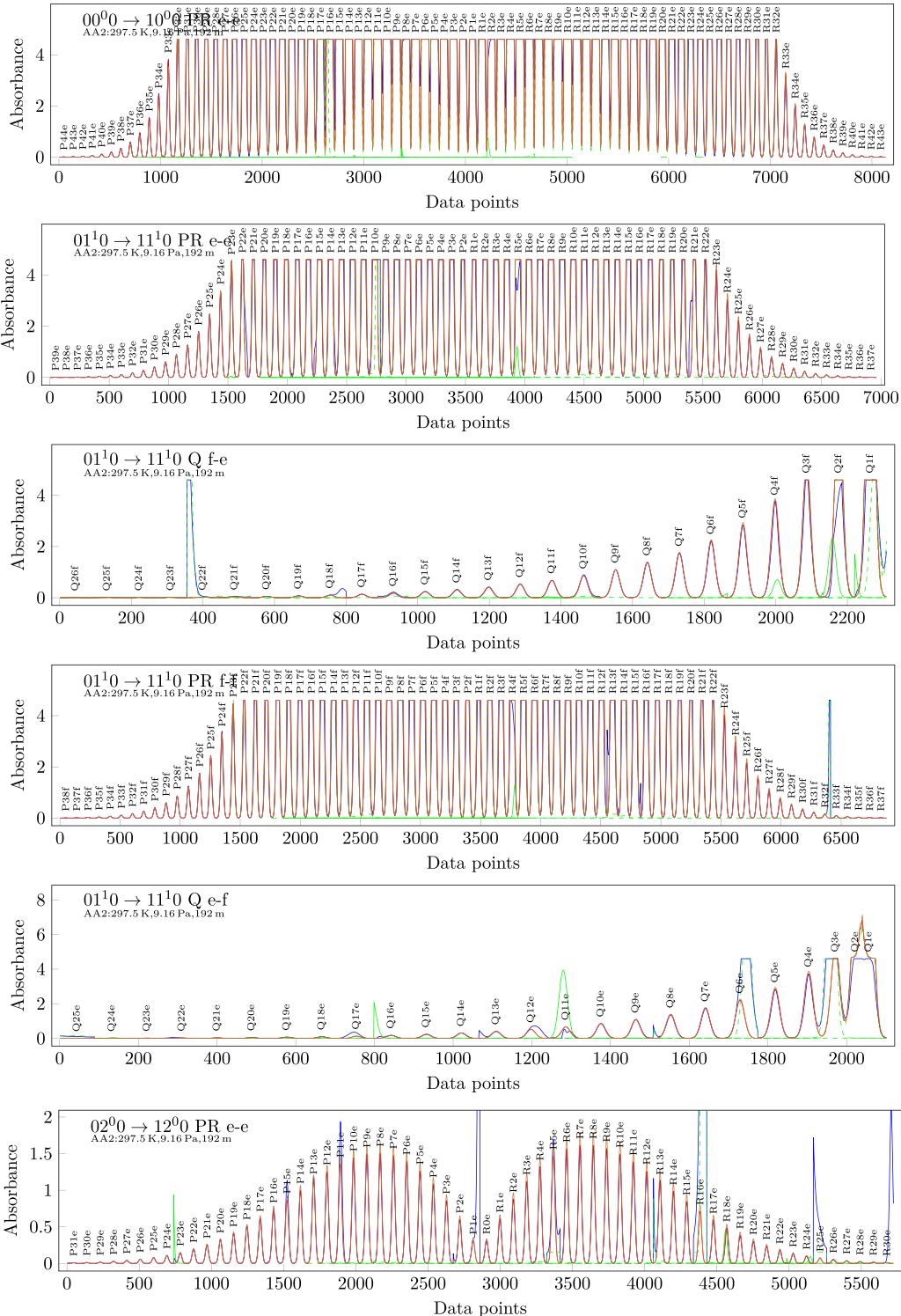


Fig. 9. Comparison between the line list of this work and an FT-IR spectrum. In these band plots, the individual lines of a subband are joined to allow a visual inspection of the line shapes. Experimental spectrum is drawn in blue, simulated spectra in red and green. Brown curves correspond to a simulation with HITRAN2016 line list. (For interpretation of the references to color in this figure legend, the reader is referred to the web version of this article.)

damental and first excited state our intensities agree with the HITRAN2016 database and the experiment better than 5%. For the higher excited states, the intensities in HITRAN2016 database are overestimated or missing, while the simulation based on the line list of this work which agrees to better than 5% with the measurements.

Fig. 11 shows the band plot and the corrected band plot of the $05^10 \rightarrow 15^10$ PR e-e subband of the emission spectrum labeled ED [39]. First, we see that the even with the extended sensitivity of 10^{-34} cm/molecule relative to the HITRAN database not all overlapping bands are simulated. The high J lines of the subband are missing due to the chosen sensitivity. The highest intensity lines in the emission spectrum are slightly suppressed due to self-absorption.

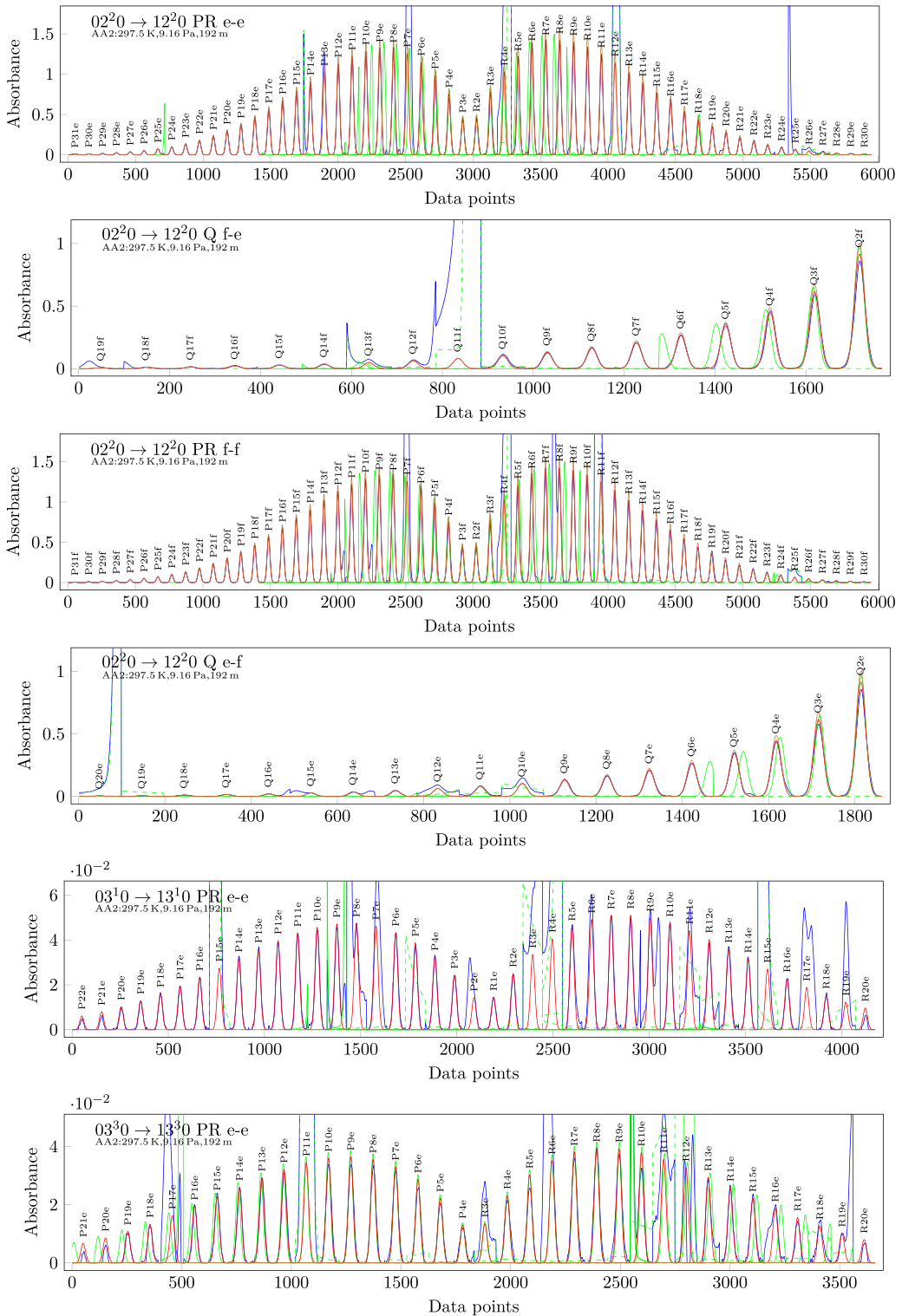


Fig. 10. Comparison between the line list of this work and an FT-IR spectrum. In these band plots, the individual lines of a subband are joined to allow a visual inspection of the line shapes. Experimental spectrum is drawn in blue, simulated spectra in red and green. Brown curves correspond to a simulation with HITRAN2016 line list. (For interpretation of the references to color in this figure legend, the reader is referred to the web version of this article.)

Again, we see a perfect match between our calculated intensity and the intensity of the lines in the experimental spectrum, this perfect agreement also holds for transitions between the highly excited states of the molecule.

In our data set, the 02^23 levels are spectroscopically predicted. There is a large difference of 25 cm^{-1} between our line positions

and those given in the HITRAN2016 database, which we assume is due to an error in HITRAN2016.

7. Linewidths

Apart from the transition wavenumbers ν_{ij} , lower state energies and intensities S_{ij} (along with quantum numbers of transitions

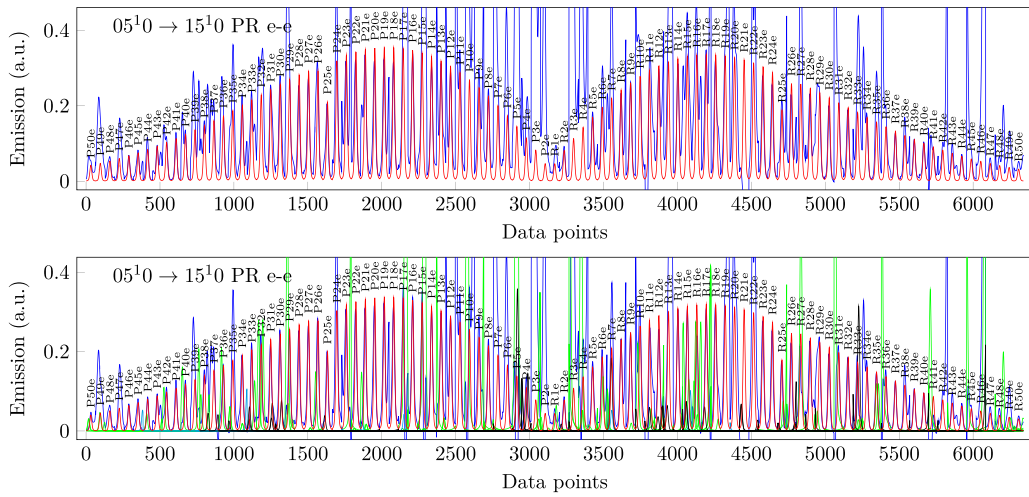


Fig. 11. Comparison between the line list of this work and an FT-IR emission spectrum. In these band plots, the individual lines of a subband are joined to allow a visual inspection of the line shapes. Experimental spectrum is drawn in blue, simulated spectra in red and green. The highest intensity lines in the emission spectrum are slightly suppressed due to self-absorption. (For interpretation of the references to color in this figure legend, the reader is referred to the web version of this article.)

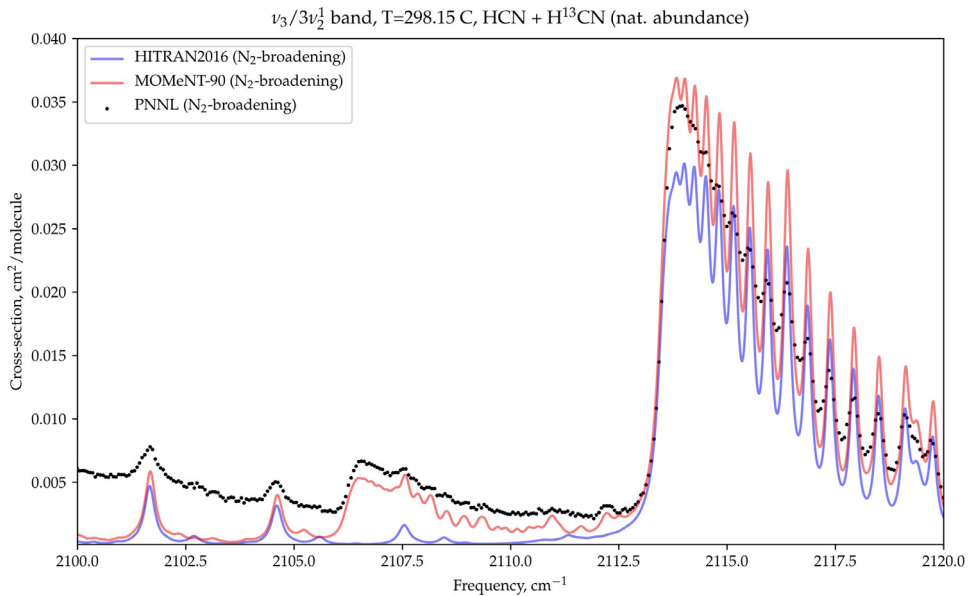


Fig. 12. Cross-section of HCN and H¹³CN (in natural abundance) from PNNL (black dots), HITRAN2016 (blue line) and MOMeNT-90 (this work) (red line) in region of ν_3 and $3\nu_2^1$ bands. The H¹³CN cross-section (from HITRAN2020 line list) was included to this work. (For interpretation of the references to color in this figure legend, the reader is referred to the web version of this article.)

states) it is necessary to have information about the line shape parameters f for modeling absorption k_{ij} in real applications, including atmospheric ones. For instance in the HITRAN database all of the transitions are given air- and self-broadened values. Additional information about definitions of the line shape parameters can be found in the HITRAN2004 paper [46] and to a wider extent on the HITRAN website (<http://www.hitran.org>).

In general, the broadening coefficients are rotationally and vibrationally dependent. However, as was shown by Yang et al. [47] for HCN, fits for states $(0, 1^1, 0)$, $(1, 0^0, 0)$ and pure-rotational states show that one can consider the vibrational dependence as negligible and use a single formula for the dependence of the broadening coefficient on the rotational number.

$$\gamma_{\text{air}}(p, T) = A_0 + A_1|m| + A_2|m|^2 + A_3|m|^3 + A_4|m|^4 \quad (3)$$

This formula was applied in HITRAN2008 [48] for all the lines with $|m| \leq 40$ (the previous polynomial used in HITRAN2004 was applicable only up to $|m| = 29$). The lines with $|m| > 40$ were assigned

a constant half-width parameter of $0.0518 \text{ cm}^{-1} \text{ atm}^{-1}$, which corresponds to the polynomial value at $|m| = 40$. Since there is no evidence for pronounced vibrational dependence of the widths for the case of HCN so this is used for all the bands.

The form given in Eq. (3) is also used for γ_{self} and n_{air} . Coefficients for these constants were taken from HITRAN2004 paper [46]. As for δ_{air} , there are only limited measurements available and there currently not enough data for all bands represented in this work so we decided to not include this parameter.

In the future it would be productive to employ Pade approximants to be able to extrapolate the trend to the rotational quanta larger than 40. As demonstrated in Refs. [49,50] Pade approximants have better predictive abilities than polynomials and therefore do not require using a constant value beyond experimental values.

In this work we used PNNL spectra [51] to validate the line list, including the line-broadening parameters. Because PNNL spectra are N₂-broadening, Eq. (3) was used with nitrogen-associated parameters also derived from Yang et al. [47]. We used the HITRAN

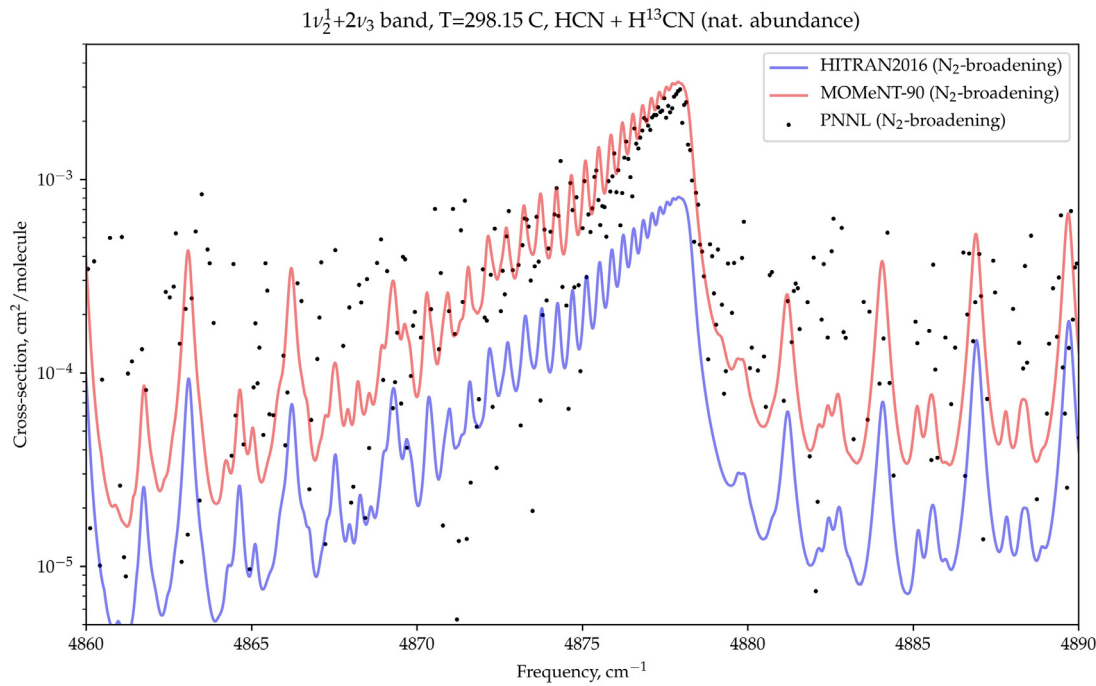


Fig. 13. Cross-section of HCN and H^{13}CN (in natural abundance) from PNNL (black dots), HITRAN2016 (blue line) and MOMeNT-90 (this work)(red line) in region of $\nu_2^1 + 2\nu_3$ band. The H^{13}CN cross-section (from HITRAN2020 line list) was included to this work. (For interpretation of the references to color in this figure legend, the reader is referred to the web version of this article.)

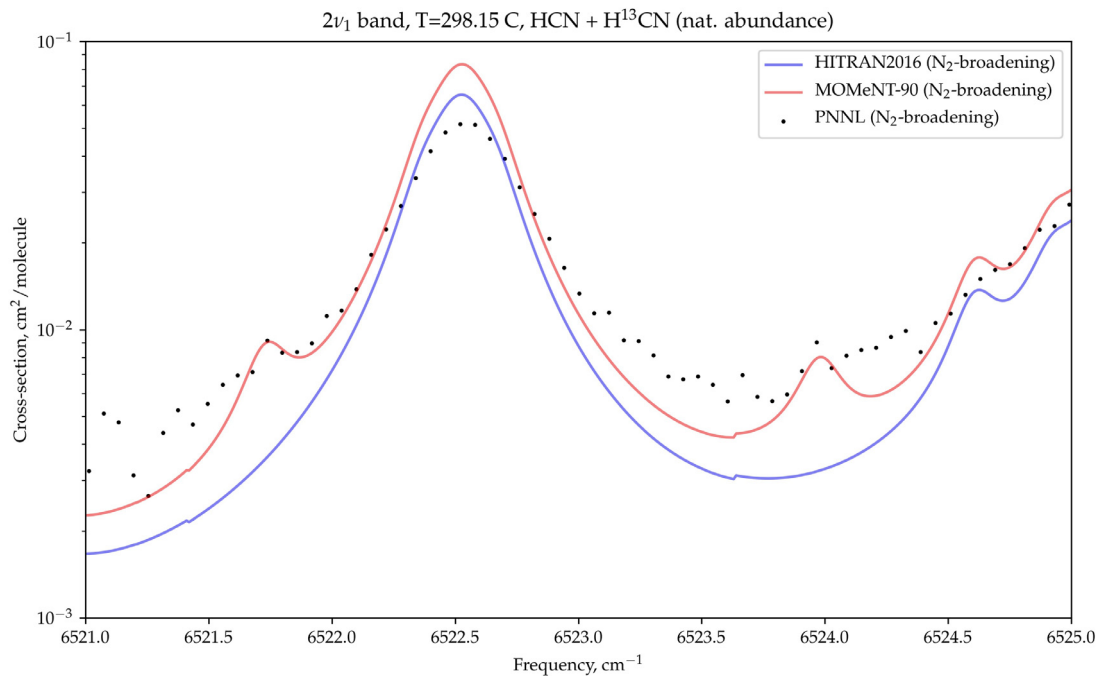


Fig. 14. Cross-section of HCN and H^{13}CN (in natural abundance) from PNNL (black dots), HITRAN2016 (blue line) and MOMeNT-90 (this work)(red line) in region of $2\nu_1$ band. The H^{13}CN cross-section (from HITRAN2020 line list) was included to this work. (For interpretation of the references to color in this figure legend, the reader is referred to the web version of this article.)

Application Programming Interface (HAPI) [52] to model the cross-sections. There are some examples of comparison PNNL spectra with modeled in this work (Figs. 12–15). For demonstration purposes we also took H^{13}CN line-list from upcoming HITRAN2020 [53] edition and add its absorption at the natural abundance. One should note that the line-mixing is not included for HCN therefore in some of the Q-branches one should not expect complete

agreement between generated cross-sections and the pressure-broadened spectrum.

As one can see from the Figures very good agreement is generally observed. For example, the region of ν_3 and $3\nu_2^1$ bands is presented on Fig. 12, where part of absorption listed in PNNL is underestimated by HITRAN2016 line list. We note that the peaks the simulated cross-sections are considerably higher than those of the PNNL cross-sections in the $2114\text{--}2120 \text{ cm}^{-1}$ region of Fig. 12. This

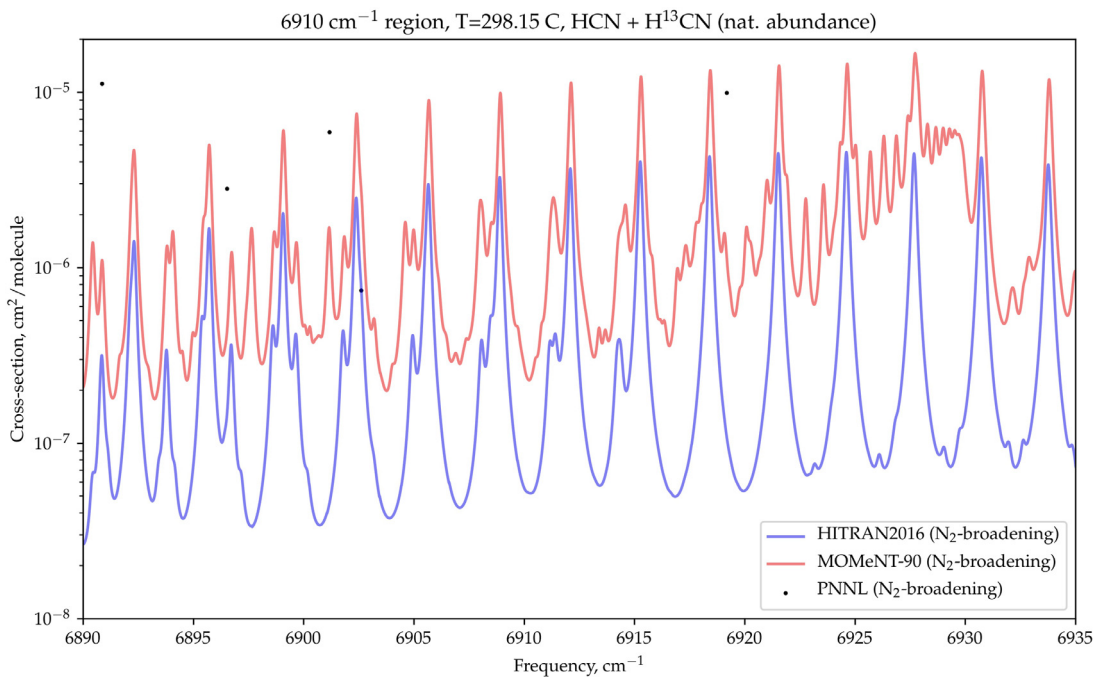


Fig. 15. Cross-section of HCN and H¹³CN (in natural abundance) from PNNL (black dots), HITRAN2016 (blue line) and MOMeNT-90 (this work) (red line) in region near 6910 cm⁻¹. The H¹³CN cross-section (from HITRAN2020 line list) was included to this work. (For interpretation of the references to color in this figure legend, the reader is referred to the web version of this article.)

region corresponds to the Q-branch of the 3ν₂ band. The intensities of this branch are very sensitive to which DMS was used in the calculations, so some of them may be slightly overestimated by our calculations. But those transitions from Q-branch, which cause the most absorption, give the best match between the PNNL and our spectra.

The discrepancy between the PNNL spectra and the HITRAN2016 data is more noticeable in the lower absorption regions, as shown in Fig. 13. Due to the weakness of the spectrum, the signal-to-noise ratio is lower here, making the band structure less clear. But it should be noted that its strongest part, the Q-band, is distinguishable and available for reliable comparison, as shown in Fig. 13.

In addition to differences in intensities, differences in absorption may be due to missing isotopologue bands (Fig. 14) or weak bands (Fig. 15).

8. Conclusion

The very accurate MOMeNT-90 line list for the rovibrational spectrum of room temperature H¹²C¹⁴N for the region below 7500 cm⁻¹ is presented. A unique attribute of this polyatomic line list comes from the fact that all the line positions, even for the very weak lines that are hardly observable experimentally, were derived from the experimental energy levels obtained from the corresponding high-temperature studies [23,33,39,41,54].

The wavefunctions obtained with the new version of the spectroscopically-tuned *ab initio* PES were used together with our accurate DMS to calculate accurate HCN line intensities at room temperature with a sensitivity of 10⁻³⁴ cm/molecule. We demonstrated the accuracy of the line intensities using some selected absorption and emission spectra. Our new intensities are very different from the intensity data present in HITRAN2016.

The creation of a hybrid line list requires an accurate mapping procedure of the theoretical line positions to the experimental ones. We think that our special mapping procedure is error-free

and we were able to detect all such misassignments present in HITRAN2016.

We provide band-by-band tables for all HCN transitions reported in this work. This dataset should support spectroscopic band-by-band analysis with our line list.

A recent scientific white paper [55] signed by 82 members of the exoplanet community describes the need for atomic and molecular data for exoplanet research. The infrared line positions for important exoplanetary molecules such as HCN are required to be accurate to 0.1 km s⁻¹, which corresponds to 0.01 cm⁻¹ for a transition at 10 000 cm⁻¹. There is also a need for data over extended temperature ranges well beyond the room temperature data contained in the HITRAN [15] and GEISA [16] databases. Our future work in the context of spectroscopic databases will be to extend the current line list to a true “hot” list for accurate spectroscopic analysis of hot HCN.

Declaration of Competing Interest

The authors declare that they have no known competing financial interests or personal relationships that could have appeared to influence the work reported in this paper.

Acknowledgments

This work was funded by RFBR through research projects number 18-02-00705 and 18-32-00698, ERC Advanced Investigator Project 883830 and the UK Natural Environment Research Council grant NE/T000767/1. OLP and GCM acknowledge the support of the Alexander von Humboldt Stiftung for the support of OLP visit to Giessen during the work on this paper. RF State Project 0030-2021-0016 is also acknowledged.

Supplementary material

Supplementary material associated with this article can be found, in the online version, at doi:[10.1016/j.jqsrt.2021.107666](https://doi.org/10.1016/j.jqsrt.2021.107666).

References

- [1] Pumphrey HC, Glatthor N, Bernath PF, Boone CD, Hannigan J, Ortega I, et al. MLS measurements of stratospheric hydrogen cyanide during the 2015–16 El Niño event. *Atmos Chem Phys Discuss* 2017;2017:1–18.
- [2] Lellouch E, Bézard B, Strobel DF, Björaker GL, Flasar FM, Romani PN. On the HCN and CO₂ abundance and distribution in Jupiter's stratosphere. *Icarus* 2006;184(2):478–97. doi:10.1016/j.icarus.2006.05.018.
- [3] Lellouch E, Romani PN, Rosenqvist J. The vertical distribution and origin of HCN in Neptune's atmosphere. *Icarus* 1994;108(1):112–36. doi:10.1006/icar.1994.1045.
- [4] Molter EM, Nixon CA, Cordiner MA, Serigano J, Irwin PGJ, Teanby NA, et al. ALMA observations of HCN and its isotopologues on titan. *Astrophys J* 2016;152:42. doi:10.3847/0004-6256/152/2/42.
- [5] Hirota T, Yamamoto S, Kawaguchi K, Sakamoto A, Ukita N. Observations of HCN, HNC, and NH₃ in comet Hale-Bopp. *Astrophys J* 1999;520:895–900. doi:10.1086/307507.
- [6] Lippi M, Villanueva GL, DiSanti MA, Boehnhardt H, Mumma MJ, Bonev BP, et al. A new model for the ν_1 vibrational band of HCN in cometary comae, with application to three comets. *Astron Astrophys* 2013;551:A51. doi:10.1051/0004-6361/201219903.
- [7] Wirström ES, Lerner MS, Källström P, Levinsson A, Olivefors A, Tegehall E. HCN observations of comets C/2013 R1 (Lovejoy) and C/2014 Q2 (Lovejoy). *Astron Astrophys* 2016;588:A72. doi:10.1051/0004-6361/201527482.
- [8] Hirota T, Yamamoto S, Mikami H, Ohishi M. Abundances of HCN and HNC in dark cloud cores. *Astrophys J* 1998;503:717–28. doi:10.1086/306032.
- [9] Eriksson K, Gustafsson B, Jørgensen UG, Nordlund A. Effects of HCN molecules in carbon star atmospheres. *Astron Astrophys* 1984;132:37–44.
- [10] van Loon JT, Marshall JR, Cohen M, Matsuura M, Wood PR, Yamamura I, et al. Very large telescope three micron spectra of dust-enshrouded red giants in the large magellanic cloud. *Astron Astrophys* 2006;447:971–89. doi:10.1051/0004-6361/20054222.
- [11] Carr JS, Najita JR. Organic molecules and water in the inner disks of T tauri stars. *Astrophys J* 2011;733:102. doi:10.1088/0004-637X/733/2/102.
- [12] Tsiaras A, Rocchetto M, Waldmann IP, Tinetti G, Varley R, Morello G, et al. Detection of an atmosphere around the super-Earth 55 Cancri e. *Astrophys J* 2016;820:99. doi:10.3847/0004-637X/820/2/99.
- [13] Hawker GA, Madhusudhan N, Cabot SHC, Gandhi S. Evidence for multiple molecular species in the hot Jupiter HD 209458b. *Astrophys J Lett* 2018;863:L11. doi:10.3847/2041-8213/aac49d.
- [14] Cabot SHC, Madhusudhan N, Hawker GA, Gandhi S. On the robustness of analysis techniques for molecular detections using high-resolution exoplanet spectroscopy. *Mon Not R Astron Soc* 2019;482:4422–36. doi:10.1093/mnras/sty2994.
- [15] Gordon IE, Rothman LS, Hill C, Kochanov RV, Tan Y, Bernath PF, et al. The HITRAN 2016 molecular spectroscopic database. *J Quant Spectrosc Radiat Transf* 2017;203:3–69. doi:10.1016/j.jqsrt.2017.06.038.
- [16] Jacquinot-Husson N, Armane R, Scott NA, Chédin A, Crépeau L, Boutammine C, et al. The 2015 edition of the GEISA spectroscopic database. *J Mol Spectrosc* 2016;327:31–72. doi:10.1016/j.jms.2016.06.007.
- [17] Rothman LS, Gordon IE, Barber RJ, Dothe H, Gamache RR, Goldman A, et al. HITEMP, the high-temperature molecular spectroscopic database. *J Quant Spectrosc Radiat Transf* 2010;111:2139–50.
- [18] Hargreaves RJ, Gordon IE, Rothman LS, Tashkun SA, Perevalov VI, Lukashewska AA, et al. Spectroscopic line parameters of NO, NO₂, and N₂O for the HITEMP database. *J Quant Spectrosc Radiat Transf* 2019;232:35–53. doi:10.1016/j.jqsrt.2019.04.040.
- [19] Tennyson J, Yurchenko SN, Al-Refaie AF, Clark VHJ, Chubb KL, Conway EK, et al. The 2020 release of the ExoMol database: molecular line lists for exoplanet and other hot atmospheres. *J Quant Spectrosc Radiat Transf* 2020;255:107228. doi:10.1016/j.jqsrt.2020.107228.
- [20] Jørgensen UG, Almlöf J, Gustafsson B, Larsson M, Siegbahn P. CASSCF and CCI calculations of the vibrational band strengths of HCN. *J Chem Phys* 1985;83:3034–42.
- [21] Harris GJ, Polyansky OL, Tennyson J. Opacity data for HCN and HNC from a new *ab initio* linelist. *Astrophys J* 2002;578:657–63. doi:10.1086/342318.
- [22] van Mourik T, Harris GJ, Polyansky OL, Tennyson J, Császár AG, Knowles PJ. *ab initio* global potential, dipole, adiabatic and relativistic correction surfaces for the HCN/HNC system. *J Chem Phys* 2001;115:3706–18. doi:10.1063/1.1383586.
- [23] Mellau GC. Complete experimental rovibrational eigenenergies of HCN up to 6880 cm⁻¹ above the ground state. *J Chem Phys* 2011;134:234303.
- [24] Harris GJ, Tennyson J, Kaminsky BM, Pavlenko YV, Jones HRA. Improved HCN/HNC linelist, model atmospheres synthetic spectra for WZ Cas. *Mon Not R Astron Soc* 2006;367:400–6.
- [25] Harris GJ, Larmer FC, Tennyson J, Kaminsky BM, Pavlenko YV, Jones HRA. A H¹³CN/HN¹³C linelist, model atmospheres and synthetic spectra for carbon stars. *Mon Not R Astron Soc* 2008;390:143–8.
- [26] Barber RJ, Strange JK, Hill C, Polyansky OL, Mellau GC, Yurchenko SN, et al. ExoMol line lists—III. An improved hot rotation-vibration line list for HCN and HNC. *Mon Not R Astron Soc* 2014;437:1828–35. doi:10.1093/mnras/stt2011.
- [27] Tennyson J, Kostin MA, Barletta P, Harris GJ, Polyansky OL, Ramanilal J, et al. DVR3D: a program suite for the calculation of rotation-vibration spectra of triatomic molecules. *Comput Phys Commun* 2004;163:85–116.
- [28] Mellau G, Winnewisser M. High S/N FT-IR emission setup for the range 300–11000 cm⁻¹. Fifteenth colloquium on high-resolution molecular spectroscopy, Glasgow, Scotland; 1997.
- [29] Mellau G, Winnewisser M, Maki A. Emission spectrum of HCN at 1400 K in the region of bending fundamental. Fifteenth colloquium on high-resolution molecular spectroscopy, Glasgow, Scotland; 1997.
- [30] Quapp W, Hirsch M, Mellau GC, Klee S, Winnewisser M, Maki A. Climbing the bending vibrational ladder in D¹³C¹⁵N by hot gas emission spectroscopy. *J Mol Spectrosc* 1999;195(2):284–98.
- [31] Maki AG, Mellau GC, Klee S, Winnewisser M, Quapp W. High-temperature infrared measurements in the region of the bending fundamental of H¹²C¹⁴N, H¹²C¹⁵N, and H¹³C¹⁴N. *J Mol Spectrosc* 2000;202:67–82. doi:10.1006/jmsp.2000.8113.
- [32] Quapp W, Melnikov V, Mellau GC. The bending vibrational ladder of H¹³C¹⁵N by hot gas emission spectroscopy. *J Mol Spectrosc* 2002;211(2):189–97.
- [33] Mellau GC, Winnewisser BP, Winnewisser M. Near infrared emission spectrum of HCN. *J Mol Spectrosc* 2008;249:23–42. doi:10.1016/j.jms.2008.01.006.
- [34] Mellau GC. Complete experimental rovibrational eigenenergies of HNC up to 3743 cm⁻¹ above the ground state. *J Chem Phys* 2010;133:164303. doi:10.1063/1.3503508.
- [35] Mellau GC. The ν_1 band system of HNC. *J Mol Spectrosc* 2010;264:2–9. doi:10.1016/j.jms.2010.08.001.
- [36] Mellau GC. Highly excited rovibrational states of HNC. *J Mol Spectrosc* 2011;269:77–85.
- [37] Makhnev VY, Kyuberis AA, Polyansky OL, Mizus II, Tennyson J, Zobov NF. A new spectroscopically-determined potential energy surface and *ab initio* dipole moment surface for high accuracy HCN intensity calculations. *J Mol Spectrosc* 2018;353:40–53. doi:10.1016/j.jms.2018.09.002.
- [38] Makhnev VY, Kyuberis AA, Zobov NF, Lodi L, Tennyson J, Polyansky OL. High accuracy *ab initio* calculations of rotation-vibration energy levels of the HCN/HNC system. *J Phys Chem A* 2018;122:1326–43. doi:10.1021/acs.jpca.7b10483.
- [39] Mellau GC. The ν_1 band system of HCN. *J Mol Spectrosc* 2011;269:12–20. doi:10.1016/j.jms.2011.04.010.
- [40] Mizus II, Kyuberis AA, Zobov NF, Makhnev VY, Polyansky OL, Tennyson J. High accuracy water potential energy surface for the calculation of infrared spectra. *Philos Trans R Soc Lond A* 2018;376:20170149. doi:10.1098/rsta.2017.0149.
- [41] Mellau GC, Kyuberis AA, Polyansky OL, Zobov N, Field RW. Saddle point localization of molecular wavefunctions. *Sci Rep* 2016;6:33068. doi:10.1038/srep33068.
- [42] Polyansky OL, Bielska K, Ghysels M, Lodi L, Zobov NF, Hodges JT, et al. High accuracy CO₂ line intensities determined from theory and experiment. *Phys Rev Lett* 2015;114:243001. doi:10.1103/PhysRevLett.114.243001.
- [43] Maki A, Quapp W, Klee S, Mellau GC, Albert S. Infrared transitions of (HCN)-C-12-N-14 and (HCN)-C-12-N-15 between 500 and 10,000 cm⁻¹. *J Mol Spectrosc* 1996;180:323–36. doi:10.1006/jmsp.1996.0255.
- [44] Schostag J. Intensity analysis of transitions between highly excited rovibrational states. Justus-Liebig-University Giessen; 2011. Master thesis.
- [45] Devi VM, Benner DC, Smith MAH, Rinsland CP, Sharpe SW, Sams RL. A multispectrum analysis of the ν_1 band of H¹²C¹⁴N: part I. Intensities, self-broadening and self-shift coefficients. *J Quant Spectrosc Radiat Transf* 2003;82:319–41. doi:10.1016/S0022-4073(03)00161-4. The HITRAN Molecular Spectroscopic Database: Edition of 2000 Including Updates of 2001.
- [46] Rothman LS, Jacquemart D, Barbe A, Benner DC, Birk M, Brown LR, et al. The HITRAN 2004 molecular spectroscopic database. *J Quant Spectrosc Radiat Transf* 2005;96:139–204.
- [47] Yang C, Buldyreva J, Gordon IE, Rohart F, Cuisset A, Mouret G, et al. Oxygen, nitrogen and air broadening of HCN spectral lines at terahertz frequencies. *J Quant Spectrosc Radiat Transf* 2008;109(17–18):2857–68.
- [48] Rothman LS, Gordon IE, Barbe A, Benner DC, Bernath PF, Birk M, et al. The HITRAN 2008 molecular spectroscopic database. *J Quant Spectrosc Radiat Transf* 2009;110:533–72.
- [49] Tan Y, Kochanov RV, Rothman LS, Gordon IE. Introduction of water-vapor broadening parameters and their temperature-dependent exponents into the HITRAN database: Part I—CO₂, N₂O, CO, CH₄, O₂, NH₃, and H₂S. *J Geophys Res* 2019;33(3). doi:10.1029/2019JD030929. 2019JD030929
- [50] Hashemi R, Gordon IE, Tran H, Kochanov RV, Karlovets EV, Tan Y, et al. Revising the line-shape parameters for air- and self-broadened CO₂ lines toward a sub-percent accuracy level. *J Quant Spectrosc Radiat Transf* 2020;256:107283. doi:10.1016/j.jqsrt.2020.107283. <https://linkinghub.elsevier.com/retrieve/pii/S0022407320304751>
- [51] Sharpe SW, Johnson TJ, Sams RL, Chu PM, Rhoderick GC, Johnson PA. Gas-phase databases for quantitative infrared spectroscopy. *Appl Spectrosc* 2004;58:1452–61. doi:10.1366/0003702042641281.
- [52] Kochanov RV, Gordon IE, Rothman LS, Wcislo P, Hill C, Wilzewski JS. HITRAN Application Programming Interface (HAPI): a comprehensive approach to working with spectroscopic data. *J Quant Spectrosc Radiat Transf* 2016;177:15–30. doi:10.1016/j.jqsrt.2016.03.005.
- [53] Gordon IE, et al. The HITRAN2020 molecular spectroscopic database. *J Quant Spectrosc Radiat Transf* 2021 In this issue.
- [54] Mellau GC. Rovibrational eigenenergy structure of the [H,C,N] molecular system. *J Chem Phys* 2011;134:194302. doi:10.1063/1.3590026.
- [55] Fortney JJ., Robinson T.D., Domagal-Goldman S., Del Genio A.D., Gordon I.E., Gharib-Nezhad E., et al. The need for laboratory measurements and *ab initio* studies to aid understanding of exoplanetary atmospheres. 2019. arXiv:1905.07064